 https://doi.org/10.3311/PPee.17676

Periodica Polytechnica Electrical Engineering and Computer Science, 65(4), pp. 382–393, 2021

Performance Assessment of Integrating SMES and Battery Storage Systems with Renewable DC-bus Microgrids: A Comparison

Kotb M. Kotb[1,2*], Mahmoud F. Elmorshedy[2], András Dán[1]

[1] Department of Electric Power Engineering, Faculty of Electrical Engineering and Informatics, Budapest University of Technology and Economics, H-1521 Budapest, P.O.B. 91, Hungary
[2] Electrical Power and Machines Engineering Department, Faculty of Engineering, Tanta University, 31521 Tanta, Egypt
* Corresponding author, e-mail: kotb.mohamed@f-eng.tanta.edu.eg

Received: 12 December 2020, Accepted: 02 March 2021, Published online: 21 September 2021

Abstract

The presence of renewable energy sources in hybrid renewable energy systems is considered a significant challenge since the generation mainly depends on meteorological conditions. Hence, employing a robust and flexible energy storage system is, therefore, a crucial solution in such circumstances. This paper investigates the performance evaluation of both batteries and superconducting magnetic energy storage (SMES) systems integrated with hybrid solar-wind DC-bus microgrid. The study focuses on enhancing the system stability using both storage technologies during normal and extreme renewables instabilities like wind gusts and shadows, and sudden load variations. Moreover, the load voltage/frequency were preserved constant during the distinct instabilities using the inverter control system. Productive findings showed the superior performance of utilizing the SMES over the batteries and its potential to enhance the system power-quality.

Keywords

battery storage system, superconducting magnetic energy storage (SMES), renewable energy systems, MPPT, wind gust

1 Introduction

Recently, exploiting the distinct renewable energy resources (RERs) has been industrialized to become one of the most significant energy sources for numerous numbers of applications due to their crucial role in reducing the need to the fossil fuels, lessening the greenhouse gases, keeping the global warming below the limits, and alleviating the climate change effects [1]. RERs have been extensively engaged to support the traditional energy resources for supplying domestic [2, 3], commercial [4] and industrial loads [5] in a microgrid (MG) structure. The MG conception, which is offered by the Consortium for Electric Reliability Technology Solutions [6], can be described as a local structure which comprises both conventional and RERs, controllable electrical and thermal loads, and an energy storage element. These microgrids are classified based on their structure to AC-bus MGs, DC-bus MGs, and hybrid MGs [7]. The DC-bus structure eliminates the complexity drawbacks and challenges of frequency stability and reactive power control in the AC-bus type. Also, the dc system losses are decreased due to the absence of skin effect, therefore, cables of smaller cross section area can be utilized. Moreover, the DC-bus MG offers straightforward management and coordination among system elements in the grid-tie operation as there is no necessity for synchronization with the main grid [8]. Unluckily, the major challenges of the DC-bus MGs are associated to grounding and protection system. The main features, limitations, and applications of each configuration can be found in [7, 9, 10]. MGs integrating energy storage systems (ESSs) have been grown to be an auspicious element for smart grids implementation [11]. Nevertheless, owing to the intermittent nature of RERs and the unpredictable load profiles, the MG every so often fails to alleviate the load demands and produces undesired instability [12]. Consequently, ESSs are utilized to smooth out the unpredictable behavior of renewable energy sources (RESs) to provide a robust and high-power quality supply. ESSs are exceedingly demanded with the developments of electrification using RESs in both grid-connected and standalone MGs to alleviate the

Cite this article as: Kotb, K. M., Elmorshedy, M. F., Dán, A. "Performance Assessment of Integrating SMES and Battery Storage Systems with Renewable DC-bus Microgrids: A Comparison", Periodica Polytechnica Electrical Engineering and Computer Science, 65(4), pp. 382–393, 2021. https://doi.org/10.3311/PPee.17676

energy transfer during normal and abnormal operation conditions; hence, the system steadiness has a substantial impact on the whole energy system through saving the extra energy during off-peak periods [13].

A diversity of energy storage technologies are employed currently in the energy market such as flywheel, pumped-hydro storage, battery storage systems (BSSs), superconducting magnetic energy storage (SMES), fuel cells, and supercapacitors (SCs) [13, 14]. Electrochemical energy storage such as BSSs are extensively relevant for numerous applications in energy sector since they have high energy density and available in different capacities, which is the major merit of this technology [15]. Various drawbacks of the BSSs incorporate voltage, current, and life-cycle limitations [16]. Mechanical storage systems such as flywheels, comprised-air, and gravity energy storage systems can operate adroitly to transform and conserve energy from resources, also they can provide the stored energy when needed for mechanical work [17]. In electrical storage technologies like SCs and SMES, energy can be stored by adjusting electric field using capacitors or magnetic fields by superconducting magnets [18]. These kinds of ESSs are characterized by the fast response, high efficiency, and long life-cycle [19]. For the SMES system, energy is kept in the form of magnetic field using the current circulation in a superconducting coil, and released back when necessary using a particular power converter [13]. To lessen the coil's ohmic loss, it is retained in a superconductive state, thus, SMES systems are classified into two types; high-temperature systems that operate at around −203 °C and low-temperature ones that operates at around −266 °C [13].

Numerous investigations have addressed the performance of different ESSs in different MG systems, however, to the best of authors knowledge, limited studies were carried out to evaluate the ESSs integration in standalone DC-bus MGs. In [3], authors mitigated the impact of RERs intermittency on the performance of a wind turbine (WT)-PV-BSS DC-bus MG using maximum power point tracking (MPPT) approaches, a DC-bus controller, and a fixed modulation index control. In [20], the performance of lithium-ion batteries integrated with a wind-PV energy system to supply inductive loads in a DC-bus MG was investigated, however, the impact of intermittent RERs was not addressed. Authors in [21] presented a global regulation control for both DC-bus and load voltages and a MPPT approach for a PV-BSS MG system to supply constant power loads, however, they studied only single type of RERs and ESSs. In [2, 8], authors integrated a controlled BSS in a PV-wind DC-bus MG and a PV-wind-diesel MG, respectively to enhance the system stability against the unpredictable behavior of RERs and loads. They also proposed a variable modulation index control method to mitigate the effect of rapid unbalanced loading. A voltage stabilization model of a wind-SMES DC-bus MG was presented in [22] to mitigate the impact of variable wind speeds by controlling the charging/discharging of the SMES unit. Another study was presented in [23] for smoothing the load Power and alleviating the DC-bus voltage of a PV-SMES-diesel DC-bus MG using load power tracking, fuzzy logic and model predictive control approaches. To merge the merits of each ESS, different studies have addressed the hybridization between different ESSs such as BSS-SMES [24], BSS-SC [25], and fuel cell-BSS-SC [26].

From the insights of the literature, the key contributions of this study can be condensed as follow:

- Improve the productivity of both PV and wind systems by employing robust MPPT techniques to assist the operation of both BSS and SMES systems.
- Mitigating instabilities of DC-bus voltage, and load voltage/frequency and power to their desired values during the different fluctuations in RERs and load.
- Highlighting the superiority of SMES system over BSS during the above-mentioned instabilities to enhance the overall system stability.

The rest of the paper is organized as follows. Section 2 and Section 3 illustrate the problem statement and the employed methodology, respectively. Section 4 shows the system structure and components modeling while Section 5 reveals the proposed control techniques. Section 6 depicts the obtained results with corresponding discussion. Finally, conclusions are summarized in Section 7.

2 Problem statement

Since the operation of both PV and wind systems depends on the alternating nature of RERs, exploiting the maximum allowable power from these resources became a challenge. Thus, MPPT techniques are employed to continuously adapt the operating point of PV and wind systems to acquire the highest accessible power. Also, this unpredictable behavior of RERs cause instabilities in the generated powers which vary with respect to the RERs variations. Besides, the accidental variabilities of the load demand pose a poor behavior in the power exchange among the MG components. Hence, MPPT techniques and ESSs perform a crucial task to reinforce the MG stability

during different variations of RERs and load power. BSS and SMES system are considered two preferred types of ESSs especially when the MGs comprise only RESs. Robust controllers are engaged with the ESSs to control the duty cycle (DuC) of the bi-directional converter to swiftly manage the charging/discharging process to mitigate any disturbances.

3 Methodology

A variation-finding comparative methodology was chosen to explore and evaluate the stability performance of renewable DC-bus MGs integrating two different ESSs (i.e., BSS and SMES) separately. Firstly, preliminary assessment was accomplished to identify the integrated ESSs, the addressed instabilities, and the employed control techniques. It was found that the performance evaluation of two different ESSs has not been compared under the same circumstances for a single MG system. Also, the extreme variations of load demand and wind gusts have not been emphasized. Secondly, robust controllers were designed for each system element to ensure exploiting the maximum possible energy from RERs, supervising, enhancing, and alleviating instabilities of system active power, preserving the MG stability, and upholding the load voltage/frequency constant during various circumstances. Thirdly, by integrating both BSS and SMES system individually into the MG, the impact of intermediate and extreme variations in renewable resources and load demand were inspected. Finally, the performance of both ESSs were analyzed and compared to reveal the effectiveness of each ESS in boosting the MG overall performance.

4 System structure and specifications

A hybrid PV-wind generation scheme integrated with ESS is considered in the study, see Fig. 1. Each component of the system is described and modelled as follows.

4.1 The PV system

A PV array of 6-kW capacity is utilized to convert the solar energy directly to electricity, the array terminals are connected to a boost converter that matches the voltages of the array and the DC-bus. Besides, it executes the employed MPPT using the control approach discussed in Subsection 5.1. The utilized PV array is a SunPower SPR-305-WHT type which has the parameters listed in Table 1.

4.2 The wind system

The employed WT is a vertical-axis type coupled with a permanent magnet synchronous generator (PMSG).

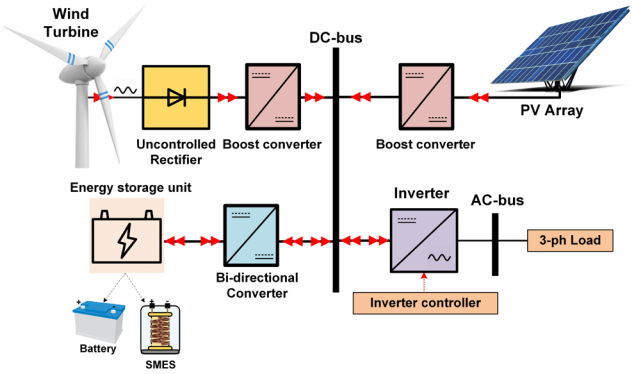

Fig. 1 Structure of the examined DC-bus MG system

Table 1 Specifications of the utilized PV module

Parameter	Value
OC voltage and SC current	321 V – 18.4 A
Max. PowerPoint parameters (V_{mp} – I_{mp})	273.5 V – 22.32 A
Parallel strings - Series modules/string	4 – 5

The generated three-phase voltage is rectified through a three-phase uncontrolled rectifier and then regulated using a boost converter to match the dc-bus voltage. This boost converter is also responsible to acquire the maximum power from the wind energy in the permissible wind speed the WT can work through. The utilized wind system parameters are listed in Table 2.

4.3 The energy storage systems

Since the studied system is entirely sustainable, incorporating energy storage device become essential to mitigate the instabilities of RERs and supervisor the energy exchanging in the system. In this study, both BSS and SMES systems are integrated individually in the DC-bus MG to highlight the substantial features and downsides of each device in this kind of MGs structure.

4.3.1 Battery storage system

A generic model of the battery is employed in this study in which the battery state of charge (SOC) is deemed as a state

Table 2 Specifications of the utilized wind system

Wind turbine		PMSG	
Parameter	Value	Parameter	Value
Nominal power	7.5 kW	Nominal power	6 kW
Cut-in speed	4 m/sec	Nominal speed	153 rad/sec
Cut-off speed	12 m/sec	Nominal current	12 A
Blade Radius	3.2 m	Nominal torque	40 N·m
Inertia	7.5 kg·m^2	Stator inductance	8.4 mH
Friction coeff.	0.06 N·m·s/rad	Armature resistance	0.4 Ω

variable to forestall the arithmetic loop difficulty and enable signifying four kinds of batteries involving the lead-acid type [27]. The battery representation uses a controlled voltage source with a constant resistance as depicted in Eqs. (1) and (2) [27] where E is the no-load voltage, E_0 is the battery constant voltage, P_v is the polarization voltage, C_{BSS} is the battery capacity, $\int i_{BSS}dt$ is the actual battery charge, A is the exponential zone amplitude, B is the exponential zone time constant inverse, V_{BSS} is the battery voltage, R_i is the internal resistance, and i_{BSS} is the battery current.

$$E = E_0 - \frac{P_v C_{BSS}}{C_{BSS} - \int_0^t idt} + A\exp\left(-B\int_0^t i_{BSS}dt\right) \quad (1)$$

$$V_{BSS} = E - R_i.I_{BSS} \quad (2)$$

A 50 Ahr lead-acid battery is integrated with the PV-wind system to supply a 6-kW load demand. The battery capacity can be determined using Eq. (3) [28] where ($E_{d/hr}$) is the energy delivered to the load demand in one hour, and (DoD) is the battery depth of discharge. In the current study, V_{BSS} = 200 V and DoD = 0.6.

$$C_{BSS} = \frac{E_{d/hr}}{V_{BSS} * DoD} \quad (3)$$

4.3.2 SMES system

A typical SMES unit consists of three basic elements: a superconducting coil, a power conditioning system, and a refrigeration and vacuum system [28]. The coil is fabricated using a superconducting material like Mercury or Niobium–Titanium. By keeping the coil at a very low temperature, its resistance become nearly zero, hence, the energy can be stored with almost zero losses [28]. In this study, a small-scale SMES unit of 120 kJ with an initial current of 350 A, 2 H inductance is connected to the DC-bus through a bi-directional dc-dc converter (Bi-DConv). The stored energy in Joules is explained in Eq. (4) while the stored/released power in Watts is presented in Eq. (5) [29]:

$$E_{SM} = 0.5I_{SM}^2 L_{SM}, \quad (4)$$

$$P_{SM} = \frac{dE_{SM}}{dt} = V_{SM} I_{SM}. \quad (5)$$

5 Proposed control techniques

The employed controllers play a curial rule in the overall system performance which significantly impacts the anticipated seeks. The distinct control methods applied for the system components are discussed as follows.

5.1 The PV system controller

The incremental conductance method (ICM) utilizes the critical set rule of derivatives on the PV output power. The description of the ICM is illustrated by Eqs. (6) and (7).

$$\frac{dP_{PV}}{dV_{PV}} = 0 \rightarrow I_{PV} + V_{PV}\frac{dI_{PV}}{dV_{PV}} = 0 \quad (6)$$

$$\frac{dI_{PV}}{dV_{PV}} = -\frac{I_{PV}}{V_{PV}} \quad (7)$$

To acquire the maximum power from the PV, both the terms of Eq. (7) must have the same magnitude with a different sign. The PV array voltage and current are measured continuously and then differentiated to the time as shown in Fig. 2. Considering a typical P-V curve of a PV module, if Eq. (6) = zero, hence, the operating point of the PV system is exactly at the top of the P-V curve (i.e., at the maximum power point). In this case, the PV voltage and current are recorded as the maximum power point parameters (V_{mp} and I_{mp} respectively), see Table 1. If Eq. (6) ≠ zero, this implies that the PV voltage is higher/lower than V_{mp}, hence, the controller decides the direction of internal perturbation to push the operating point in the direction of the top of the P-V curve. Therefore, the sign of Eq. (6) determines the location of the operating point. If the sign is positive, hence, the operating point located on the right of the maximum power point (the PV voltage is greater than V_{mp}). If the sign is negative, hence, the operating point located on the left of the maximum power point (the PV voltage is lower than V_{mp}). Therefore, the MPPT controller start adjusting the DuC of the boost converter, till satisfying Eq. (6), to drive the operating point in the direction of the maximum power point. Fig. 2 describes the MPPT controller of the PV system.

5.2 The wind system controller

A typical wind system delivers a no-load rated output power as in Eq. (8) [2]. The generation from the wind energy

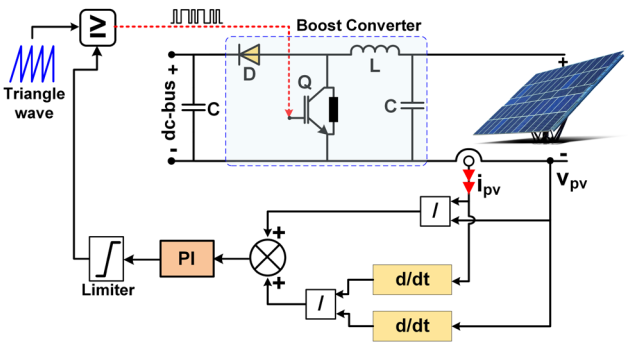

Fig. 2 MPPT of the PV system

depends on the air density (ρ), the rotor swept area (A), the cubic wind speed (V_w^3), and the wind power-coefficient (C_p) which is attained by Eq. (9) [30]. The coefficients c_a–c_g can be found in [2].

$$P_w = 0.5\,\rho A V_w^3 C_p \tag{8}$$

$$C_p(\lambda,\beta) = C_a\left(\frac{C_b}{\lambda_i} - C_c\beta - C_d\right)e^{\frac{C_f}{\lambda_i}} + C_g\lambda \tag{9}$$

$$\frac{1}{\lambda_i} = \frac{1}{\lambda + 0.08\beta} - \frac{0.035}{\beta^3 + 1}, \quad \lambda = \frac{R\omega_r}{V_w} \tag{10}$$

A MPPT based on the wind speed measurement method [2] is engaged in this study in which the wind power-coefficient is defined by Eqs. (9) and (10). The power-coefficient mainly depends on the tip-speed ratio (λ) and the pitch angle (β). The $(C_p$–$\lambda)|_{\beta=0}$ is displayed in Fig. 3 in which it can be remarked that there is a certain value of λ at which the power-coefficient is maximum (C_{popt}); this value is defined as the optimum tip-speed ratio (λ_{opt}). Hence, to preserve the tip-speed ratio at its optimum value, the rotor speed (ω_r) should be adjusted together with the wind speed variation. Once the maximum power coefficient is obtained, optimal (maximum) power can be obtained from the wind turbine (P_{wmax}).

The MPPT of the wind system is shown in Fig. 4 in which the optimal wind power P_{wmax} is compared with the actual power produced by the wind turbine (P_w). The controller determines the DuC of the boost converter under distinct wind speeds. In order to handle the maximum value of the PMSG current, specific limiters are employed in the control system.

5.3 The BSS controller

The BSS controller has two key functions; to alleviate the DC-bus voltage during the operation instabilities and

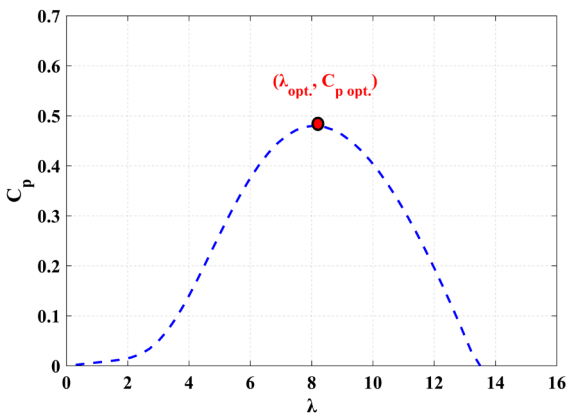

Fig. 3 The C_p–λ characteristics of a wind turbine at $\beta = 0$

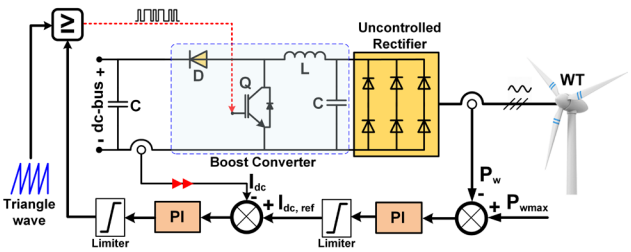

Fig. 4 MPPT of the wind system

to control the power flow in the system. The behavior of the load rms voltage follows the behavior of the DC-bus voltage, therefore, it is essential to maintain the bus voltage constant during the operation. The operation mode of the BSS is decided based on how far the DC-bus voltage from the reference value is. When the generated power become greater than the load demand, the DC-bus voltage surpasses the reference value. The control system begin to reduce the voltage through the DuC of the buck-boost converter and the BSS start charging. Conversely, in the discharging operation, when the generated power become not adequate to fulfil the load demand, the DC-bus voltage drops below the reference value. Therefore, the control system start to boost the voltage by controlling the DuC, and the battery begins to discharge to overcome the occurring deficiency. The BSS controller is illustrated in Fig. 5 in which the battery current is measured and compared with the reference current which is determined depends on the behavior of the DC-bus voltage. The control system generates the DuC required to buck or boost the DC-bus voltage to its reference value.

5.4 The SMES system controller

The SMES coil is charged or discharged using the Bi-DConv which is moderated to supply positive or negative voltage

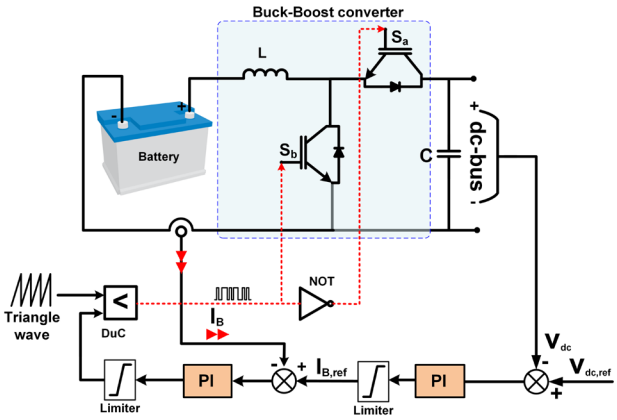

Fig. 5 Control system of the BSS

to the SMES coil as illustrated in Fig. 6. When S_1 and S_2 are turned ON, positive voltage is then supplied from the MG to the SMES coil (charging mode). When S_1 and S_2 are turned OFF, negative voltage is applied on the SMES coil which means that the stored energy is discharged from the coil to the MG through diodes D_1 and D_2. Changing the average voltage across the SMES coil is defined by DuC of the Bi-DConv. When the DuC is greater than 0.5 and less than 1, energy is stored into the coil while for DuC less than 0.5, the stored energy is released to the dc-bus. When the DuC exactly equal 0.5, the stored energy circulates in either (S_1-D_2-coil) or (D_1-S_2-coil) loops and hence, the SMES stays in a stand-by mode. The previous control sequence is moderated via two consecutives PI-controllers as displayed in Fig. 7. The first one handles the DC-bus voltage error and defines the SMES reference current for the second PI-controller. To generate the gate signals of S_1 and S_2, the DuC is compared with a triangular signal.

5.5 The inverter system controller

Since it is essential to isolate the load voltage/frequency away from instabilities caused by RERs or load demand as possible, a typical 3-phase, 3-legs inverter is utilized and controlled in a way to simultaneously achieve this target. The line voltages of the load can be calculated using Eq. (11) [2] which indicate that the line voltages can be regulated based on the DC-bus voltage and the phase modulation index $m_{ph,x}$ where the subscript x refers to the phases (a, b, or c). The control circuit of the inverter is shown in Fig. 8. The rms value of each phase is compared with the reference value; based on the behavior of each phase, a particular modulation index is generated from the multipliers stage. Based on the modulation index, proper switching pulses are created to keep the load voltage/frequency constant. The employed control method has the advantage of handling instabilities caused by the sudden loading-unbalance.

$$V_{L-L} = 0.6123\, m_{ph,x}\ \ V_{DC-bus} \tag{11}$$

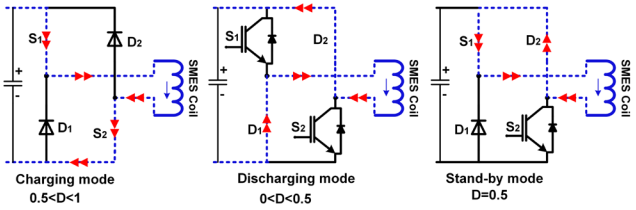

Fig. 6 Different modes of operation of the SMES

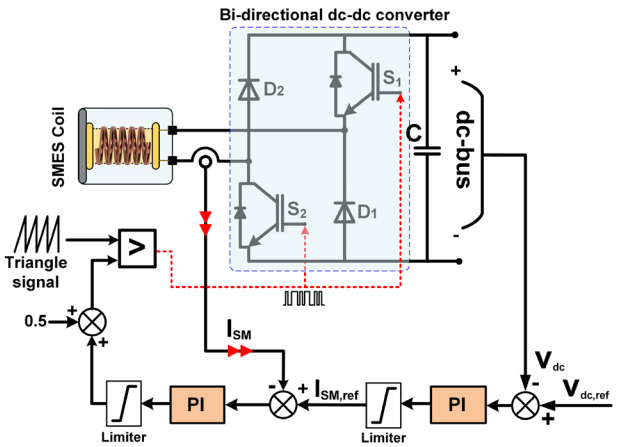

Fig. 7 The SMES control unit

6 Results and discussion

Based on the main focus of this study, a comparison between the SMES and the BSS has been conducted under the same operating conditions. It is worth to mention that, in all the investigated cases, the wind turbine is connected to the MG system at t = 5 s to examine the performance of the two ESSs in alleviating the WT connection consequences. The different instabilities are examined and analyzed as follows.

6.1 Case-1: Moderate variation of RERs

In this case, the system performance is examined by varying both wind speed and solar radiation as shown in Fig. 9. Firstly, the MPPT control methods of both PV and wind systems are efficiently executed during the variations of wind speed and solar radiation as indicated in Fig. 10 and Fig. 11, respectively. It can be recognized from Fig. 12 that the proposed control systems effectively upheld the DC-bus voltage during the variations. It was observed that the proposed control systems using SMES is superior compared to the BSS which is reflected also on the load

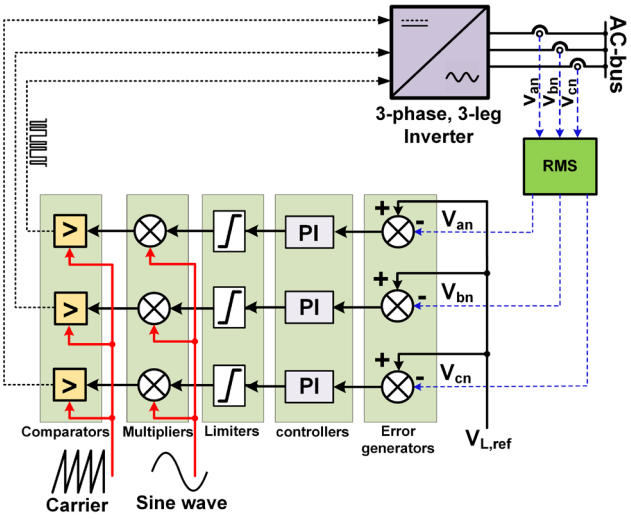

Fig. 8 Control circuit of the 3-phase, 3-leg inverter

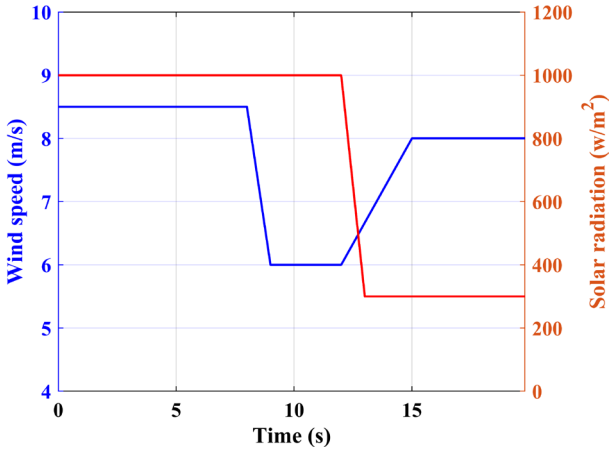

Fig. 9 Variation of RERs in case-1

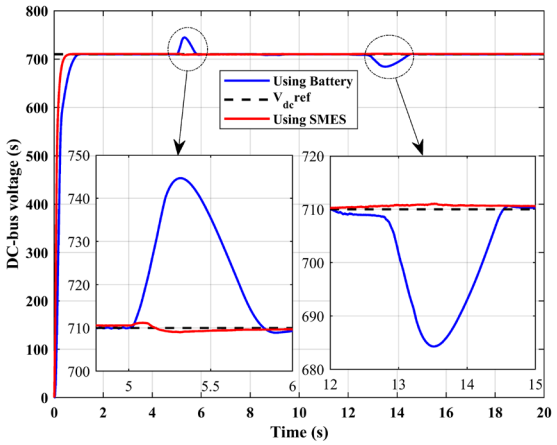

Fig. 12 The DC-bus voltage during case-1

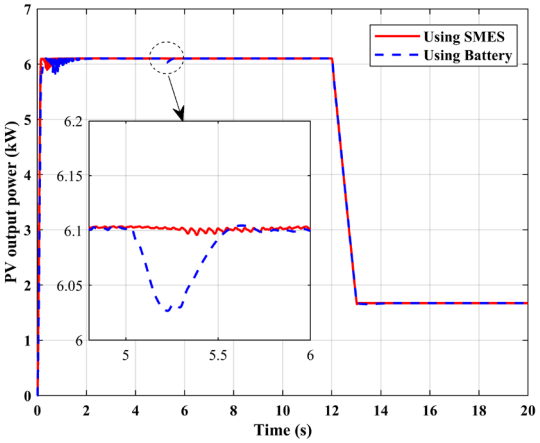

Fig. 10 The PV generated power during case-1

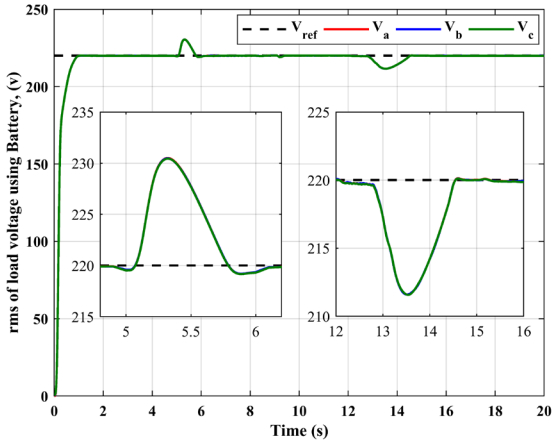

Fig. 13 Load rms voltage using BSS during case-1

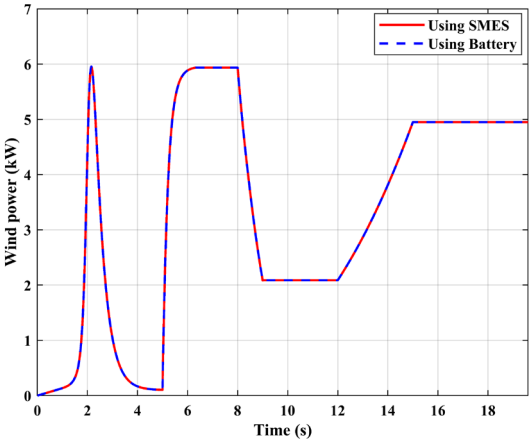

Fig. 11 The wind generated power during case-1

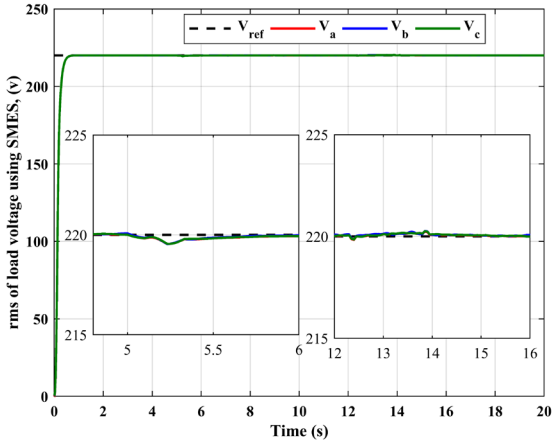

Fig. 14 Load rms voltage using SMES during case-1

rms voltage, load instantaneous voltage and frequency, and load power as illustrated in Figs. 13 to 16.

6.2 Case-2: Loading variation

In this case, the load profile is changed as follows: 8.54 kW (0 s to 8 s), then decreased to 5.8-kW (8 s to 15 s), and finally increased to 10.37 kW (15 s to 20 s). During the load variation, both wind speed and solar radiation are assumed constant at 8.5 m/s and 1000 w/m^2, respectively. In Fig. 17, it can be seen that the response time and the capability to mitigate the load instabilities of the SMES is superior compared to the BSS. Moreover, the proposed control methods using

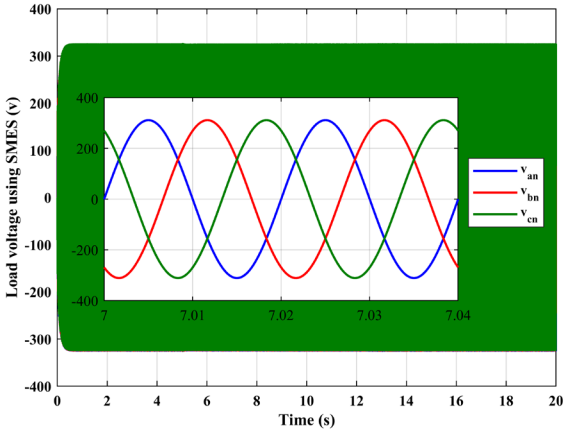

Fig. 15 Instantaneous load voltage using SMES during case-1

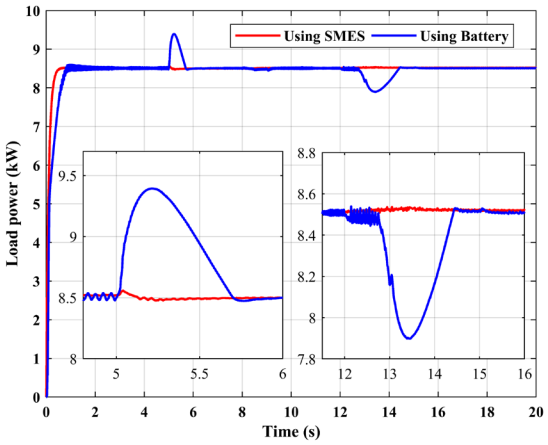

Fig. 16 The delivered load power during case-1

SMES efficiently retained the DC-bus voltage, load rms voltage constant compared to the BSS as shown in Figs. 18 to 20. The power-sharing in the MG during this case is also illustrated in Fig. 21 which verifies the effectiveness of the control methods using both the SMES and BSS. Besides, the behavior of both the SMES and BSS in terms of energy, currents and SOC is displayed in Figs. 22 and 23.

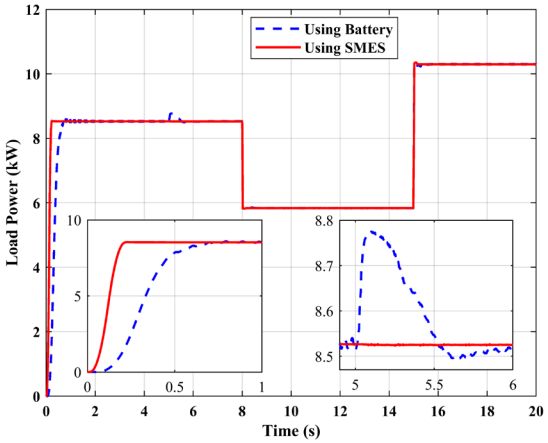

Fig. 17 The delivered load power during case-2

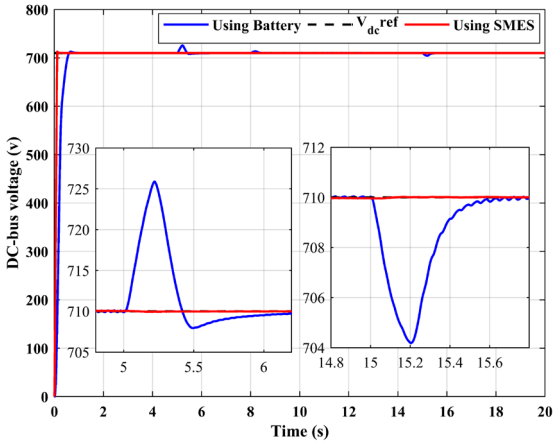

Fig. 18 The DC-bus voltage during case-2

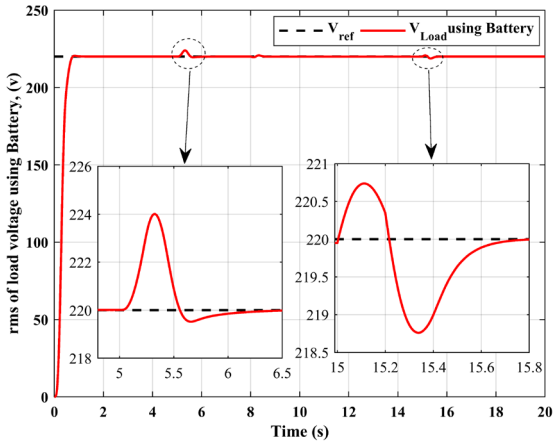

Fig. 19 Load rms voltage using BSS during case-2

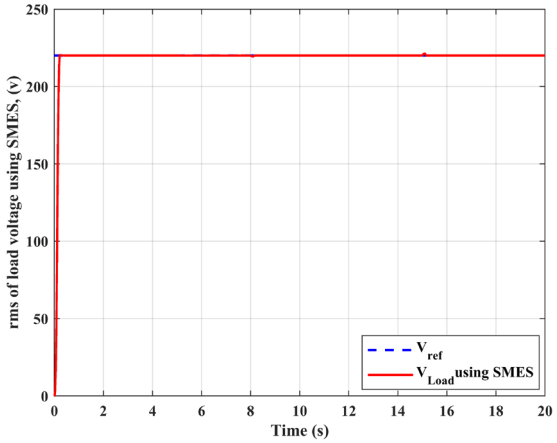

Fig. 20 Load rms voltage using SMES during case-2

6.3 Case-3: Extreme variations of RERs

This case is considered as the worst-case where a wind gust and shadow are occurring simultaneously while the load power remains constant at 8.5 kW. The RERs profile which depict this case is illustrated in Fig. 24. The proposed control methods magnificently maintained the DC-bus and load rms voltages steady with a superior

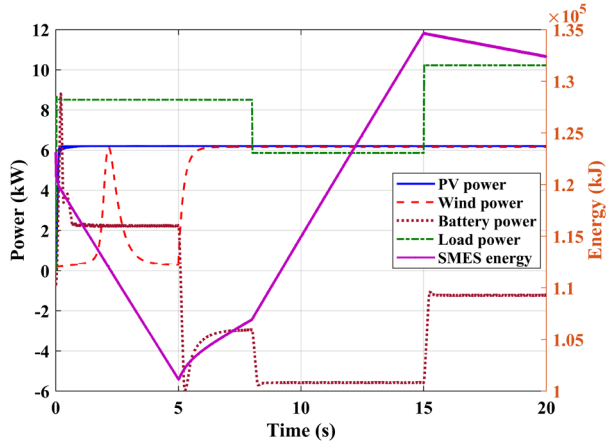

Fig. 21 Powe and energy sharing during case-2

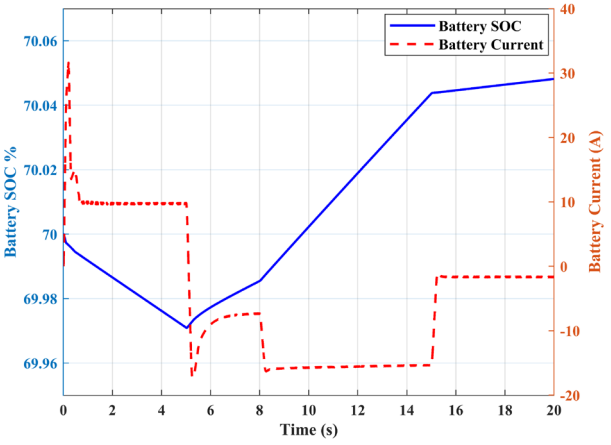

Fig. 22 Battery SOC and current during case-2

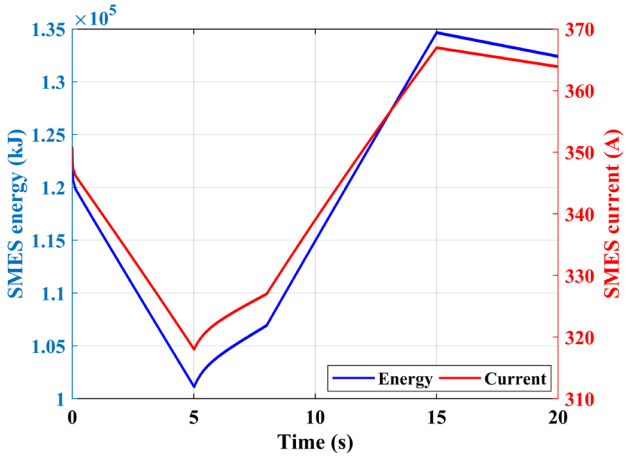

Fig. 23 SMES energy and current during case-2

accomplishment of the SMES compared to the BSS which has a large undershoot during disturbances as seen in Figs. 25 and 26. Moreover, the comportment of both the SMES and BSS in terms of energy, currents and SOC is displayed in Figs. 27 and 28.

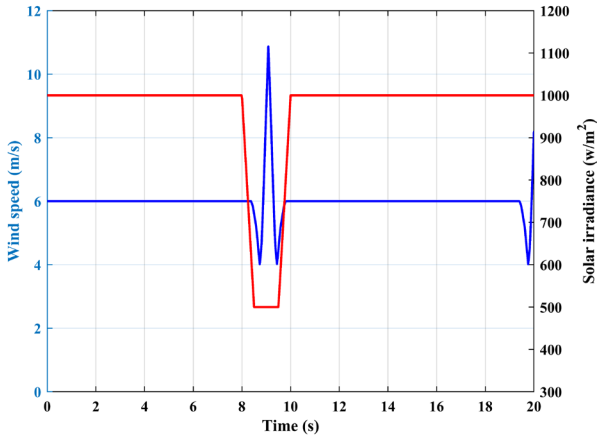

Fig. 24 RERs profile during case-3

Finally, the instantaneous load voltage using both SMES and BSS is displayed in Figs. 29 and 30 in which the effectiveness of using SMES system over BSS is clearly indicated.

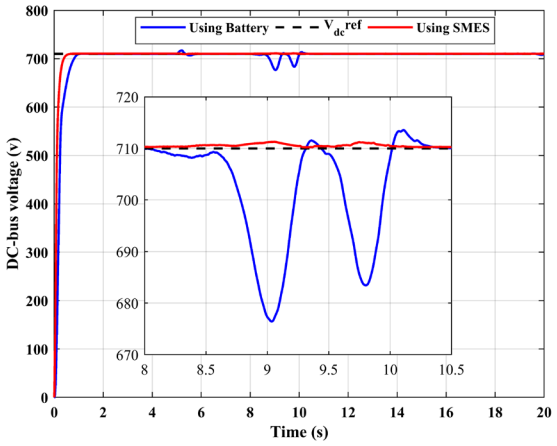

Fig. 25 The DC-bus voltage during case-3

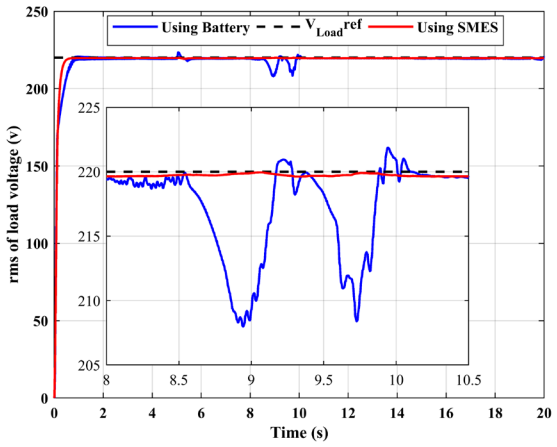

Fig. 26 The load rms voltage during case-3

7 Conclusion

This work examined a comparison between the performance of the BSS and SMES technologies integrated with

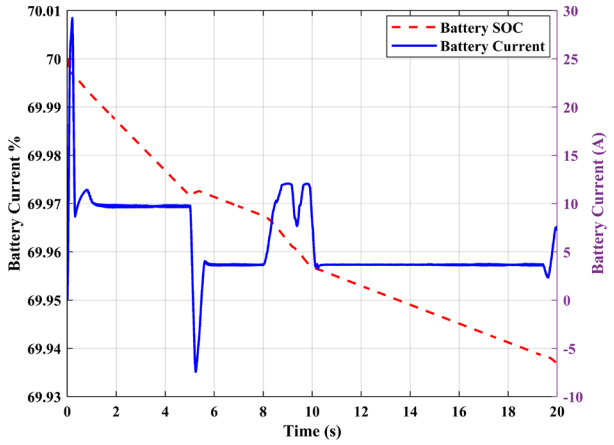

Fig. 27 Battery SOC and current during case-3

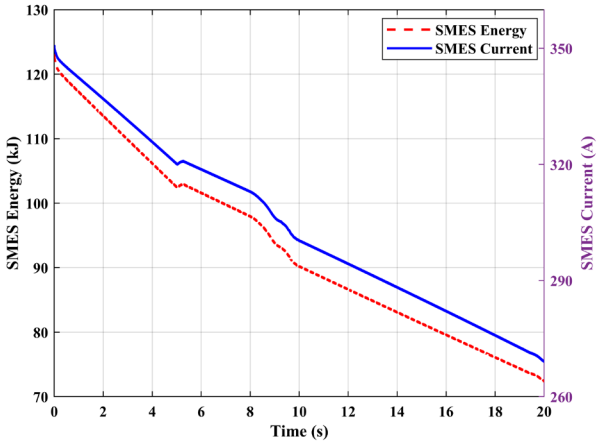

Fig. 28 SMES energy and current during case-3

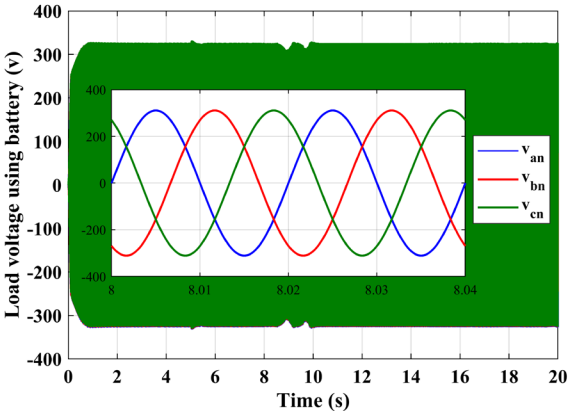

Fig. 29 Instantaneous load voltage using the BSS during case-3

hybrid renewable DC-bus microgrid system. Developed control approaches for acquiring the maximum power

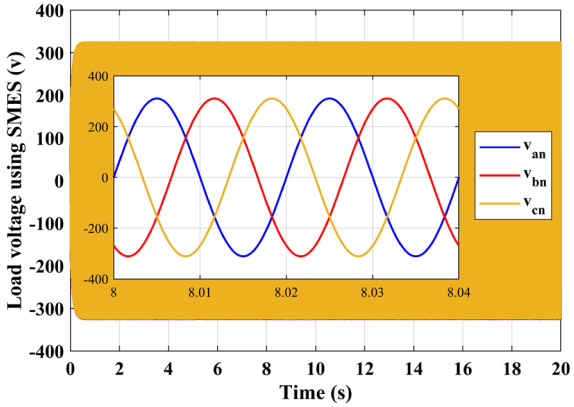

Fig. 30 Instantaneous load voltage using the SMES during case-3

from both solar and wind energies were presented. These MPPT approached strengthened the performance of the proposed control methods of BSS, SMES, and the inverter for regulating voltages and power exchange during the wind gusts and load variations. The power transferred between the DC-bus and BSS or SMES coil was controlled with the proposed control circuit of the bi-directional DC-DC converters. The controllers were designed to facilitate both the BSS and SMES to efficiently charge/discharge power to reimburse the instability of DC-bus voltages, load voltage and frequency, and load power. The acquired findings demonstrated the usefulness of the SMES overall performance over the BSS during the distinct instabilities in the system. The proposed control methods succeeded in alleviating both the DC-bus and load voltages and enhancing the power exchange among the PV, wind generators and load side during the extreme wind gusts and random load instabilities. The superior SMES performing transmuted the control objectives to swiftly charge/discharge energy all through the moderate and extreme wind and radiation variations and the unintentionally load variations. This, in turn, facilitated in enhancing the DC-bus and load voltages to the tolerable boundaries which validates the support of the proposed control methods. The outlook work of this study will investigate the effectiveness of employing hybrid ESSs comprises BSS and SMES or SCs. Besides, enhancing the MPPT and ESSs control techniques by applying the fuzzy environment to enhance the accuracy of controllers' outcomes.

References

[1] Zappa, W., Junginger, M., Broek, M. "Is a 100% renewable European power system feasible by 2050?", Applied Energy, 233–234, pp. 1027–1050, 2019. https://doi.org/10.1016/j.apenergy.2018.08.109

[2] Kotb, K. M., Elkadeem, M. R., Elmorshedy, M. F., Dán, A. "Coordinated power management and optimized techno-enviro-economic design of an autonomous hybrid renewable microgrid: A case study in Egypt", Energy Conversion and Management, 221, Article number: 113185, 2020. https://doi.org/10.1016/j.enconman.2020.113185

[3] Elmorshedy, M. F., Kotb, K. M., Dán, A. "Hybrid Renewable Microgrid System Based DC-bus Scheme for Residential Load Applications", In: 2019 22nd International Conference on Electrical Machines and Systems (ICEMS), Harbin, China, 2019, pp. 1–6. https://doi.org/10.1109/ICEMS.2019.8922530

[4] Zachar, M., Daoutidis, P. "Energy management and load shaping for commercial microgrids coupled with flexible building environment control", Journal of Energy Storage, 16, pp. 61–75, 2018. https://doi.org/10.1016/j.est.2017.12.017

[5] Alramlawi, M., Gabash, A., Mohagheghi, E., Li, P. "Optimal Operation of PV-Battery-Diesel MicroGrid for Industrial Loads Under Grid Blackouts", In: 2018 IEEE International Conference on Environment and Electrical Engineering and 2018 IEEE Industrial and Commercial Power Systems Europe (EEEIC / I&CPS Europe), Palermo, Italy, 2018, pp. 1–5. https://doi.org/10.1109/EEEIC.2018.8493959

[6] Tan, X., Li, Q., Wang, H. "Advances and trends of energy storage technology in Microgrid", International Journal of Electrical Power & Energy Systems, 44(1), pp. 179–191, 2013. https://doi.org/10.1016/j.ijepes.2012.07.015

[7] Justo, J. J., Mwasilu, F., Lee, J., Jung, J. W. "AC-microgrids versus DC-microgrids with distributed energy resources: A review", Renewable and Sustainable Energy Reviews, 24, pp. 387–405, 2013. https://doi.org/10.1016/j.rser.2013.03.067

[8] Kotb, K. M., Elmorshedy, M. F., Dán, A. "Permanence Improvement of a Local Energy Production System Including Unbalanced Loading", In: 2019 International IEEE Conference and Workshop in Óbuda on Electrical and Power Engineering (CANDO-EPE), Budapest, Hungary, 2019, pp. 185–190. https://doi.org/10.1109/CANDO-EPE47959.2019.9110974

[9] Unamuno, E., Barrena, J. A. "Hybrid ac/dc microgrids - Part I: Review and classification of topologies", Renewable and Sustainable Energy Reviews, 52, pp. 1251–1259, 2015. https://doi.org/10.1016/j.rser.2015.07.194

[10] Unamuno, E., Barrena, J. A. "Hybrid ac/dc microgrids - Part II: Review and classification of control strategies", Renewable and Sustainable Energy Reviews, 52, pp. 1123–1134, 2015. https://doi.org/10.1016/j.rser.2015.07.186

[11] Graditi, G., Ippolito, M. G., Telaretti, E., Zizzo, G. "An Innovative Conversion Device to the Grid Interface of Combined RES-Based Generators and Electric Storage Systems", IEEE Transactions on Industrial Electronics, 62(4), pp. 2540–2550, 2015. https://doi.org/10.1109/TIE.2014.2336620

[12] Li, J., Xiong, R., Yang, Q., Liang, F., Zhang, M., Yuan, W. "Design/test of a hybrid energy storage system for primary frequency control using a dynamic droop method in an isolated microgrid power system", Applied Energy, 201, pp. 257–269, 2017. https://doi.org/10.1016/j.apenergy.2016.10.066

[13] Faisal, M., Hannan, M. A., Ker, P. J., Hussain, A., Mansor, M. B., Blaabjerg, F. "Review of Energy Storage System Technologies in Microgrid Applications: Issues and Challenges", IEEE Access, 6, pp. 35143–35164, 2018. https://doi.org/10.1109/ACCESS.2018.2841407

[14] Hannan, M. A., Hoque, M. M., Mohamed, A., Ayob, A. "Review of energy storage systems for electric vehicle applications: Issues and challenges", Renewable and Sustainable Energy Reviews, 69, pp. 771–789, 2017. https://doi.org/10.1016/j.rser.2016.11.171

[15] Xu, X., Bishop, M., Oikarinen, D. G., Hao, C. "Application and modeling of battery energy storage in power systems", CSEE Journal of Power and Energy Systems, 2(3), pp. 82–90, 2016. https://doi.org/10.17775/cseejpes.2016.00039

[16] Alsaidan, I., Khodaei, A., Gao, W. "A Comprehensive Battery Energy Storage Optimal Sizing Model for Microgrid Applications", IEEE Transactions on Power Systems, 33(4), pp. 3968–3980, 2018. https://doi.org/10.1109/TPWRS.2017.2769639

[17] Guney, M. S., Tepe, Y. "Classification and assessment of energy storage systems", Renewable and Sustainable Energy Reviews, 75, pp. 1187–1197, 2017. https://doi.org/10.1016/j.rser.2016.11.102

[18] Kousksou, T., Bruel, P., Jamil, A., El Rhafiki, T., Zeraouli, Y. "Energy storage: Applications and challenges", Solar Energy Materials and Solar Cells, 120, pp. 59–80, 2014. https://doi.org/10.1016/j.solmat.2013.08.015

[19] Gong, K., Shi, J., Liu, Y., Wang, Z., Ren, L., Zhang, Y. "Application of SMES in the Microgrid Based on Fuzzy Control", IEEE Transactions on Applied Superconductivity, 26(3), pp. 1–5, 2016. https://doi.org/10.1109/TASC.2016.2524446

[20] Doshi, K., Harish, V. S. K. V. "Analysis of a wind-PV battery hybrid renewable energy system for a dc microgrid", Materials Today: Proceedings, 46(11), pp. 5451–5457, 2021. https://doi.org/10.1016/j.matpr.2020.09.194

[21] Sun, J., Lin, W., Hong, M., Loparo, K. A. "Voltage Regulation of DC-Microgrid with PV and Battery: A Passivity Method", IFAC-PapersOnLine, 52(16), pp. 753–758, 2019. https://doi.org/10.1016/j.ifacol.2019.12.053

[22] Shaaban, E. F., El-Wahab Hassan, A., Mansour, D.-E. A., Yuan, W. "Application of SMES for voltage stabilization of PMSG connected to DC grids", In: 2018 53rd International Universities Power Engineering Conference (UPEC), Glasgow, UK, 2018, pp. 1–5. https://doi.org/10.1109/UPEC.2018.8541934

[23] Habib, H. U. R., Wang, S., Farhan, B. S., Salih, H. W., Waqar, A., Kotb, K. M. "Load Power Smoothing and DC Bus Voltage Control of PV-SMES Standalone Microgrid based Variable Speed DG using FLC-MPC Approach", In: 2019 3rd International Conference on Energy Conservation and Efficiency (ICECE), Lahore, Pakistan, 2019, pp. 1–6. https://doi.org/10.1109/ECE.2019.8920903

[24] Sun, Q., Xing, D., Alafnan, H., Pei, X., Zhang, M., Yuan, W. "Design and test of a new two-stage control scheme for SMES-battery hybrid energy storage systems for microgrid applications", Applied Energy, 253, Article number: 113529, 2019.
https://doi.org/10.1016/j.apenergy.2019.113529

[25] Singh, P., Lather, J. S. "Power management and control of a grid-independent DC microgrid with hybrid energy storage system", Sustainable Energy Technologies and Assessments, 43, Article number: 100924, 2021.
https://doi.org/10.1016/j.seta.2020.100924

[26] Krishan, O., Suhag, S. "Grid-independent PV system hybridization with fuel cell-battery/supercapacitor: Optimum sizing and comparative techno-economic analysis", Sustainable Energy Technologies and Assessments, 37, Article number: 100625, 2020.
https://doi.org/10.1016/j.seta.2019.100625

[27] Tremblay, O., Dessaint, L., Dekkiche, A. "A Generic Battery Model for the Dynamic Simulation of Hybrid Electric Vehicles", In: 2007 IEEE Vehicle Power and Propulsion Conference, Arlington, Texas, USA, 2007, pp. 284–289.
https://doi.org/10.1109/VPPC.2007.4544139

[28] Luo, X., Wang. J., Dooner, M., Clarke, J. "Overview of current development in electrical energy storage technologies and the application potential in power system operation", Applied Energy, 137, pp. 511–536, 2015.
https://doi.org/10.1016/j.apenergy.2014.09.081

[29] Kotb, K. M., Said, S. M., Dán, A., Hartmann, B. "Stability Enhancement of Isolated-Microgrid Applying Solar Power Generation Using SMES Based FLC", In: 2019 7th International Istanbul Smart Grids and Cities Congress and Fair (ICSG), Istanbul, Turkey, 2019, pp. 104–108.
https://doi.org/10.1109/SGCF.2019.8782321

[30] Allam, S. M., Elmorshedy, M. F., Rashad, E. M. "Load power and state-of-charge management strategy with MPPT of wind-driven isolated PMSG", In: 2016 22nd International Conference on Electrical Machines (ICEM), Lausanne, Switzerland, 2016, pp. 1098–1104.
https://doi.org/10.1109/ICELMACH.2016.7732662